







Magnetic variation in construction steels under tensile stress. Empirical research with Helmholtz coils

 D. Ferrández^a,  C. Morón ,  P. Saiz^c,  A. Morón^b

a. Departamento de Ingeniería de Organización, Administración de Empresas y Estadística, Universidad Politécnica de Madrid,
Grupo Sensores y Actuadores (Madrid, Spain)

b. Departamento de Tecnologías de la Edificación, Universidad Politécnica de Madrid,
Grupo Sensores y Actuadores (Madrid, Spain)

c. Universidad Rey Juan Carlos, Departamento de Economía Financiera, Contabilidad e Idioma Moderno,
Campus de Vicálvaro (Madrid, Spain)

 carlos.moron@upm.es

Received: 10 May 2020
Accepted: 30 September 2020
Available on line: 17 March 2021

ABSTRACT: Steel is responsible for providing resistance to flexotraction to reinforced concrete structures. Steel is responsible for providing reinforced concrete structures with a flexural strength. For this reason, it is important to study its behaviour under different tensile states. This study used measuring equipment that was able to determine variations in magnetic properties of B500-SD steel bars during standard tensile tests. The magnetic field generated by a Helmholtz coil was collected through a secondary circuit. This enables the induced electromotive force to relate with the steel deflection stages when subjected to the tests. Moreover, it was possible to determine the variation of magnetic permeability when submitting 12mm and 16mm diameter bars to different tensile states. This method could prove extremely useful in determining the tensile state of ribbed steel bars that are embedded into the concrete structure.

KEYWORDS: Magnetical properties; Steel; Tensile Strength; Permeability.

Citation/Citar como: Ferrández, D.; Morón, C.; Saiz, P.; Morón, A. (2021) Magnetic Variation in Construction Steels under tensile stress. Empirical research with Helmholtz coils. Mater. Construcc. 71 [341], e243 <https://doi.org/10.3989/mc.2021.06020>

RESUMEN: *Variación magnética en aceros de construcción sometidos a esfuerzos de tracción. Investigación empírica con bobinas de Helmholtz.* El acero se encarga de dotar de resistencia a flexotracción a las estructuras de hormigón armado. Por esto, es imprescindible conocer cuál es su comportamiento cuando se encuentra sometido a distintos estados de tensión. En este trabajo se ha implementado un equipo de medida capaz de determinar las variaciones en las propiedades magnéticas de las barras de acero B500-SD cuando se someten a un ensayo de tracción normalizado. El campo magnético generado por una bobina Helmholtz ha sido recogido mediante un circuito secundario, permitiendo relacionar la fuerza electromotriz inducida con las etapas de deformación del acero durante el ensayo de tracción. Además, se ha podido determinar cómo varía la permeabilidad magnética al someter barras de diámetro 12 mm y 16 mm a distintos estados de tensión. Este método puede ser útil para conocer el estado tensional de las barras de acero cuando se encuentran dentro de una estructura de hormigón.

PALABRAS CLAVE: Propiedades magnéticas; Acero; Resistencia a la Tracción; Permeabilidad.

Copyright: ©2021 CSIC. This is an open-access article distributed under the terms of the Creative Commons Attribution 4.0 International (CC BY 4.0) License.

1. INTRODUCTION

The reinforced concrete, which is mainly formed by concrete and ribbed steel bars, is one of the most used materials in the construction sector. For this reason, it is very important to study its behaviour and its components performance, under different types of stress during the building process (1).

Steel ribbed bars provide reinforced concrete structures with higher flexural strength. The study of these materials is crucial to determine the behaviour of structures during the building process (2). Magnetism of materials is caused by magnetic moments associated to the motion of individual electrons, so that in every individual atom, orbital moments of some electronics pairs are fully cancelled, as are in spin moments. Thus, the net magnetic moment of an atom will be the vector sum of its electrons magnetic moments. On the basis of the magnetic behaviour of materials in response to external magnetic fields, we can find different types of magnetism: diamagnetism, paramagnetism and ferromagnetism (3).

For this study, and as we are dealing with steel alloys, with iron as the main component, we will work with ferromagnetic materials that are widely used in engineering because of their high magnetic susceptibilities. This means that the magnetic induction is practically proportional to the magnetization of the studied solid (4). These ferromagnetic properties may be affected by the temperature and mechanical strength. In the first case, saturation magnetization decreases with increasing temperature and it will reach the Curie temperature, where the material loses its ferromagnetic properties to be replaced by paramagnetism (5). On the other hand, the general physical characteristics can be defined in terms of magnetic constants, that is to say, the tensed steel bar varies its magnetic character according to the magnitude and force direction with respect to its limit of elasticity (6).

One of the most used configurations to reach a region of a relatively uniform magnetic field is the Helmholtz Coil. Helmholtz coils are two coaxial circular coils of the same radius. This radius is equal to the distance between the coil plains (7). Our study used standard configuration with the current circulating in the same direction through the two coils. Needless to say, the anti-Helmholtz configuration (current passing in opposite directions in both coils) has a wide field of application in biomedical studies (8).

When using this type of coils in industry, it is essential to know its intensity and uniformity and to delimit the region where the generated magnetic field is uniform. One of the most important applications of these coils is the possibility of measuring the magnetic field generated by

electronic devices, with the aim of studying its behaviour in wider systems (9). The magnetic field to be determined can be situated in the far or the near field region (10, 11). Another important application of this type of coils is the inspection of ferromagnetic tubes, such as those used in oil wells or in perforation tubes, as they can be used to detect cracks if the magnetic saturation of material is reached (12). Even though these inspection techniques are widely spread, they have a narrow field of application because of their high cost and surface cleaning requirements (13). In recent decades, corrosion monitoring of pipelines has been affected by the use of these measuring techniques. New devices have been designed in order to isolate signals and detect pitting on the pipes surface (14).

When submitting ferromagnetic material to an external magnetic field such as the one generated by a Helmholtz coil, the variation of magnetic domains is affected by the microstructure of the material and its tensile state (15). For this reason, it is possible to establish relations between the magnetic properties of certain materials such as steel and the mechanical strength to which they are subjected to. On the basis of these evidences, many authors try to establish relations between the tensile state of carbon steels and the composition in their microstructure. This microstructure is fundamental for industrial usage with non-destructive techniques based on the interpretation of the response received under the influence of an external magnetic field (16). One of the most used applications of this method is the detection of imperfections in cable-stayed bridges as it evaluates the tension in prestressing cables that are used to ensure this type of structures (17). This application is of great utility as the mechanical heterogeneities of any origin are identified in the lack of magnetic homogeneity in the magnetized material. This technique can be used with a high level of reliability for imperfections detection (18). The main difficulty in obtaining these magnetic curves lies in the complexity of signal processing, in the correction of zero displacement, and in the integration to obtain appropriate tension signals (19). For this reason, some authors have focused on harmonic and spectral analyses as a tool for simplifying filtering and softening of signals and for obtaining universal results for its application in non-destructive inspection methods (20).

The objective of this work is to determine the variation of magnetization of construction steels under longitudinal tensile stress. By using Helmholtz coils, the challenge is to establish the relation between the applied tensile stress, the deflection rate and the variation produced in the magnetization of ferromagnetic material. To achieve this, two different diameters of steel bars and measuring equipment designed by the authors were used in the tests. This will enable to calculate with a

high degree of accuracy the variations in the magnetic properties of the material.

2. MATERIALS AND METHODS

2.1. Steels used in the research

For performing the testing and following the standards UNE 36065:2011 and UNE 36068:2011 about ribbed steels for concrete (21, 22), ribbed bars made of special characteristics of ductility were used. The bars deployed were hot-rolled steel bars fabricated with continuous casting billet. They had solid circular sections, with at least two ribbed transversal rows equally distributed over its whole length. 12 and 16 mm diameter high ductility steel weldable bars, type B500SD, were cut at 500 mm of length for tensile stress tests.

Table 1 shows the required minimum mechanical characteristics for B500SD steel according to standard UNE 36065.2011.

The B500SD steel has specific chemical characteristics referred to the analysis of the chemical composition of casting and the admissible values in the analysis of the product, as shown in Table 2.

The equivalent carbon is calculated as follows (Equation [1]):

$$\%C_{eq} = \%C + \frac{\%Mn}{6} + \frac{\%Cr + \%Mo + \%V}{5} + \frac{\%Ni + \%Cu}{15} \quad [1]$$

where the symbols of chemical elements indicate its content in percentage in mass.

At the microstructural level, the B500SD steel is composed by a ferrite matrix with a substantial volume fraction of the pearlite micro-constituent (formed by a ferrite-cementite lamellar composite). The crystal structure of cementite is orthorhombic and ferrite in body-centred cubic, which are related with the magnetic domain structure on magnetization of the steel (23).

2.2. Helmholtz Coil

It is intended to show the variation of magnetic properties of concrete steels under mechanical stress. For such a purpose, it was necessary to design a coil capable of generating a strong enough magnetic field to delimit the test to the breaking zone in the ferromagnetic material.

The relation in which flow density can be calculated in any point of space where the electric current circulates is given by Biot-Savart law (Equation [2]):

$$d\vec{B} = \frac{\mu_0}{4\pi} \cdot \frac{Id\vec{l} \times \vec{a}}{a^2} \quad [2]$$

where $d\vec{B}$ is a differential element of the magnetic field generated in a plane perpendicular to the plane formed by longitudinal element $d\vec{l}$ separated at \vec{a} distance from the point of application, where I is the intensity of the current circulating through the conduct; and μ_0 is the magnetic susceptibility in a vacuum.

The configuration of the current corresponds to the Helmholtz coil, that is, two circular coils of equal radius, with a common axis, separated at such distance that the second derivative of \vec{B} is cancelled in a point of the axis situated in the center of two coils (24).

The magnetic induction at a point P indicated in Figure 1b is given by the expression (Equation [3]):

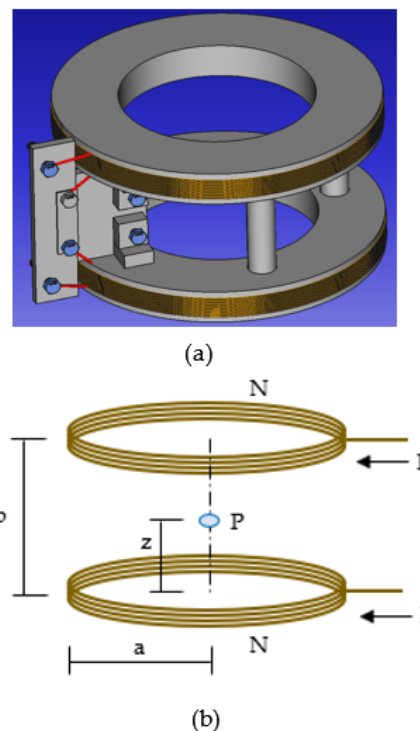


FIGURE 1. (a) Helmholtz Coil in 3D; (b) Axial field of Helmholtz coil.

TABLE 1. Required minimum mechanical standards for B500SD steel.

Yielding Limit f_y (MPa)	Ultimate Tensile Stress f_s (MPa)	Relation f_s/f_y [p]	Elongation at maximum load ϵ (%)	Break Elongation A_5 (%)
500	575	$1.15 \leq f_s/f_y \leq 1.35$	≥ 8	≥ 16

TABLE 2. Chemical composition of B500SD steel.

Element *	C (%)	S (%)	P (%)	N (%)	Cu (%)	C equivalent (%)
Casting analysis	0.22	0.05	0.05	0.012	0.8	0.5
Product analysis	0.24	0.055	0.055	0.014	0.85	0.52

* Percentages are referred to maximum permissive content.

$$B_z(z) = \frac{N\mu_0 I a^2}{2} \left\{ \frac{1}{(z^2 + a^2)^{3/2}} + \frac{1}{[(2b - z)^2 + a^2]^{3/2}} \right\} \quad [3]$$

where factor N is included to take into account the situation in which every coil has N turns; a is the radius of the coil; $2b$ indicates the separation between coils; and z the distance to the point P .

The first derivative of B_z with respect to z is (Equation [4]):

$$\frac{dB_z}{dz} = \frac{N\mu_0 I a^2}{2} \left\{ -\frac{3}{2} \left(\frac{2z}{(z^2 + a^2)^{5/2}} + \frac{2(z - 2b)}{[(2b - z)^2 + a^2]^{5/2}} \right) \right\} \quad [4]$$

As it can be observed, it is cancelled for $z = b$. The second derivative with respect to z is (Equation [5]):

$$\frac{d^2 B_z}{dz^2} = -\frac{3N\mu_0 I a^2}{2} \left\{ \frac{1}{(z^2 + a^2)^{5/2}} + \frac{1}{[(2b - z)^2 + a^2]^{5/2}} - \frac{5}{2} \left(\frac{2z^2}{(z^2 + a^2)^{7/2}} + \frac{2(z - 2b)^2}{[(2b - z)^2 + a^2]^{7/2}} \right) \right\} \quad [5]$$

for $z = b$ it is reduced to (Equation [6]):

$$\frac{d^2 B_z}{dz^2} \Big|_{z=b} = -\frac{3N\mu_0 I a^2}{2} \left\{ \frac{a^2 - 4b^2}{(b^2 + a^2)^{7/2}} \right\} \quad [6]$$

Which is cancelled if $a^2 - 4b^2 = 0$. Thus, a proper choice for b is $2b = a$, being the separation between coils equal to the radius.

With the separation mentioned above, a magnetic induction is obtained in the midpoint of (Equation [7]):

$$B_z = \frac{\mu_0 N I}{a} \frac{8}{5^{3/2}} \quad [7]$$

Nevertheless, it is convenient to know the value of the magnetic field at any point along the coil axis that is near the midpoint of the two coils and where the steel bar will be situated. In this way, the field $B_z(z)$ can be developed in Taylor series around the point $z = 1/2a$ in order to

know its intensity variations with respect to the midpoint according to the following expression (Equation [8]):

$$B_z(z) = B_z\left(\frac{1}{2}a\right) + \left(z - \frac{1}{2}a\right) \frac{\partial B_z}{\partial z} \Big|_{z=1/2a} + \dots \quad [8]$$

As the first three derivatives are cancelled, the fourth derivative $B_z(z)$ can be expressed as follows (Equation [9]):

$$B_z(z) = B_z\left(\frac{1}{2}a\right) \left\{ 1 - \frac{144}{125} \left(\frac{z - a/2}{a} \right)^4 \right\} \quad [9]$$

so for the region where $|z - a/2|$ is less than $a/10$, $B_z(z)$ presents a deviation with respect to $B_z(a/2)$ that is really small (less than 1/5 in 10000).

Thus, the configuration of the Helmholtz coil is presented as an ideal solution for establishing a specific area of a known and uniform magnetic field. In this research, this area corresponds to the breaking section of test specimens. The objective of that was to determine the influence of this mechanical stress in its magnetic properties.

2.3. Equipment designed for magnetization measuring

For the convenience of analysis, for each bar of B500SD steel, instructions established by the standard UNE EN ISO 6892-1:2017 were followed. To define this model, it is necessary to use unit deflection in z direction (longitudinal direction of the bar), that is given by the expression (Equation [10]):

$$\varepsilon = \frac{\partial l}{\partial z} \quad [10]$$

and the elastic tension defined as (Equation [11]):

$$\sigma = \frac{\mathcal{F}}{S} \quad [11]$$

where \mathcal{F} defines the tensile force in kN through a bar section, and S is the section of the bar that, for this study, varies according to the diameters of 12 mm or 16 mm.

Moreover, it is known that for unidimensional tensile states in which deflections are small, both expressions are related by the Hooke law (Equation [12]):

$$\sigma = E\varepsilon \quad [12]$$

where E is the Young modulus of steel.

Before the test, each bar was marked over its whole length with lines separated from each other by one centimetre distance. This will allow us to measure the last elongation after the tensile strength, elongation that was determined over the initial length of the specimen that was around 5 diameters (Equation [13]):

$$A_5 = \frac{L_f - L_0}{L_0} \cdot 100 \quad [13]$$

where L_f and L_0 are the initial and final length of the specimen.

These tests were performed using a hydraulic machine of IBERTEST series, with a testing capacity of 100 kN, according to the standard UNE-EN ISO 6892-1:2017. This mechanism was equipped with a extensometer of 50 mm of length that allows obtaining the stress-strain diagram.

Elasticity was controlled by the load, removing the extensometer when the deformation reached 2%. Once elasticity limit was reached, control was made by deflection. In this way, diagrams in which load was indicated in the Y-axis and elongation in the X-axis were obtained. Results also show the hydraulic press piston.

In addition, B500SD is classified as a ferromagnetic material. In these materials, the atomic magnetic moments can be ordered under the action of a magnetic field that is below its Curie temperature. This is due to the spins orientation of unpaired internal electrons.

As it can be observed in Figure 2, the pattern resistance of 1 Ω is connected in series with the primary coils in order to measure the tension and the current (25). In the secondary reel, that is formed by

the number of turns (N_S), the induced electromotive force (U_{ind}) is given as (Equation [14]):

$$U_{ind}(t) = -N_S \frac{d\phi}{dt} = -N_S \left[\mu_0 \frac{d}{dt} \int_{S_0}^{S_f} H(r,t) dS + \frac{d}{dt} \int_0^{S_f} B(r,t) dS \right] \quad [14]$$

where B is a magnetic induction over the transversal section of the material; H is the magnetic induction; μ_0 is the magnetic permeability in a vacuum; S_f is the area of transversal section of a steel bar; and S_0 is a transversal area of the detection coil (26).

This induced tension is collected by the integrating fluxmeter. In this way, the magnetic induction $B(t)$ is obtained by the integration of the $U_{ind}(t)$ signal. An analogue integrator, with an RC time constant, will provide the output voltage (Equation [15]):

$$U_{out} = -\frac{1}{RC} \int_{t_1}^{t_2} U_{ind}(t) dt = \frac{N_S}{RC} \left[\mu_0 \int_{S_0}^{S_f} \Delta H(r) dS + \int_0^{S_f} \Delta B(r) dS \right] \quad [15]$$

where $\Delta H(r)$ and $\Delta B(r)$ correspond to the variation of the intensity of magnetic field and induction respectively within the time frame (t_1, t_2).

If we consider as uniform the magnetization field in the transversal area of detection coil S_0 , its intensity H will depend only on the intensity of the tension I that circulates in the magnetizing coil. The output tension of the analogue integrator can be expressed according to the known magnetization

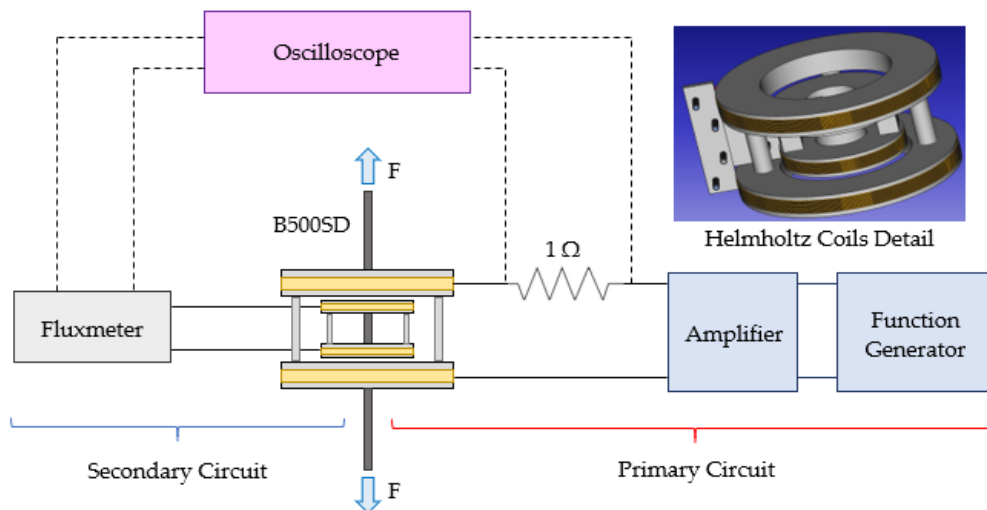


FIGURE 2. Measuring equipment scheme.

field ΔH and to the magnetic induction ΔB of the sample using the following expression (Equation [16]):

$$U_{out} = \frac{N_S}{RC} [\mu_0 (S_0 - S_f) \Delta H + S_f \Delta B] \quad [16]$$

where S_f is a transversal section area of the steel bar.

In order to obtain the magnetic amplitude permeability $\mu = \frac{B}{\mu_0 H}$ of the material, the following equation can be used (Equation [17]):

$$\mu = 1 + \frac{S_0}{S_f} \left(\frac{U_{out}}{U_0} - 1 \right) \quad [17]$$

where U_0 represents the tension obtained in the secondary circuit in a vacuum, without the steel bar.

Moreover, the magnetic induction B is not a linear function of the magnetic induction H , that is, the magnetic permeability μ is not constant. This means that there can be a flow in the steel even without the existence of an exterior field. This is caused by the ferromagnetic properties of this material. In this way, it is possible to build curves that allow studying the behaviour of μ according to H when the material is under a specific tensile stress.

3. RESULTS AND DISCUSSION

In the following section, the results of the research and the discussion of these results are presented.

3.1. Installation of the experimental equipment

Figure 3 shows the installation of the measuring equipment used in this research. The hydraulic traction machine used for standardized steel tests can be observed in the figure, as well as the scheme devices in Figure 2. It also includes a Teslameter, a device that is able to measure a magnetic field.



FIGURE 3. Measuring equipment for the tests performed in the laboratory.

3.2. Relation between the tensile stress and the induced electromotive force (emf)

Figure 4 and Figure 5 show the graphics obtained after the tensile test for the steel bars with the two studied diameters: 12 and 16 mm. The test was performed at ambient temperature, so it has no influence on the results. The sample was placed in such a way that its longitudinal axis was parallel to the direction of the tensile axis force.

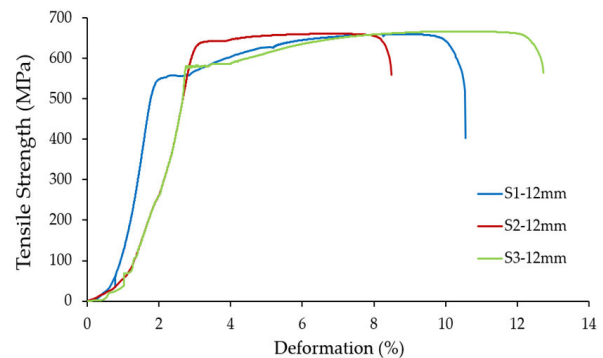


FIGURE 4. Graphics Tensile Strength (MPa) - Deformation (%). Steel bar B500-SD of 12 mm diameter.

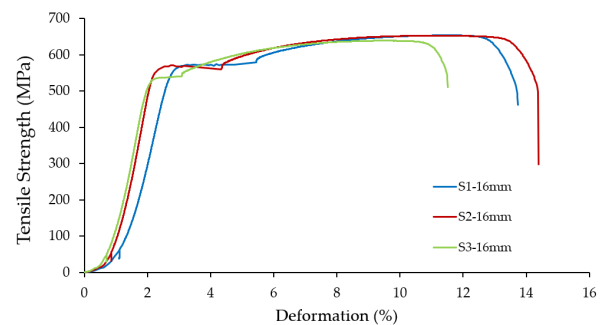


FIGURE 5. Graphics Tensile Strength (MPa) - Deformation (%). Steel bar B500-SD of 16 mm diameter.

The break of the steel bars is cup-shaped on the furthest end from the break and truncated cone-shaped on the side corresponding to the point of rupture. This is related to the 45° plans theory of break with relation to the force direction, with the particular feature of the specimen having rotational symmetry.

At the atomic level, there are differences between the behaviour in the elastic zone and the plastic zone (Figure 6). In the first instance, the atoms are maintained unified in their original structure, even though they get slightly separated. However, when the force ceases, the atoms regain their balance properties and their crystalline structure remains unchanged as it was at the beginning. On the

contrary, during the plastic stage, a lot of atoms break their original connection even though they will rejoin nearby atoms. This will generate a new crystalline structure that has similar properties to the initial one, with the difference that when the force decreases, the resulting deflection is permanent and the crystalline structure gets altered, as well as the external physical form of the material (27, 28).

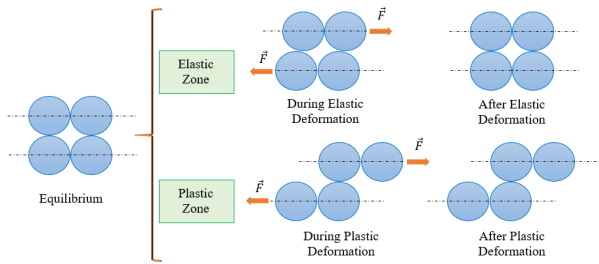


FIGURE 6. Evolution of the steel structure during progressive tensile test.

Thus, this defT produced during the test causes a variation of the induced electromotive force that is registered by the measuring equipment. The results corresponding to each bar are shown in Figure 7 and Figure 8, where colour code is maintained to facilitate the interpretation.

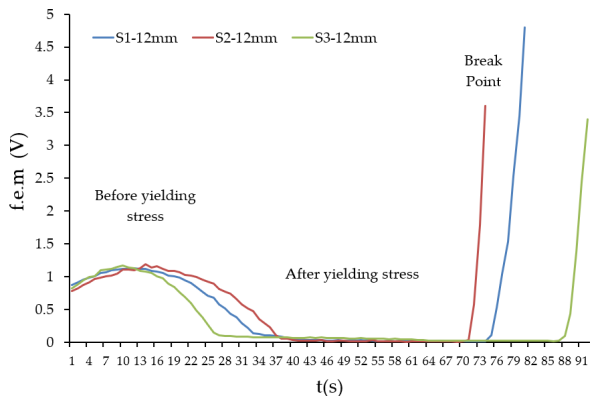


FIGURE 7. Induced Electromotive Force (V) - Time (s) during tensile test. Bar of 12 mm.

In Figure 7 and Figure 8, it can be observed how the induced electromotive force varies according to the time since the tensile force began to be applied to each bar. These curves show several well-defined areas that have their interpretation in the force-strain diagram.

In the first area, there is an increase of the induced electromotive force, that corresponds to the rise of the magnetic permeability due to the tensile force. In the second area, there is a decline of the induced electromotive force until a change in the slope of the curve is produced. This change corresponds to the unit load in the point where the deflections of the

sample are not proportional to the applied force, in other words until the yielding limit. This is the real yielding limit that can be defined as the maximum load with a momentary application that does not produce significant modifications in the dimensions of the bar nor in the physical or chemical properties of the steel.

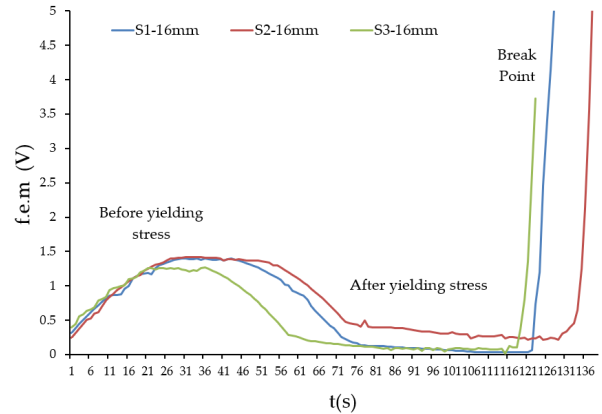


FIGURE 8. Induced Electromotive Force (V) - Time (s) during tensile test. Bar of 16 mm.

The third area corresponds to the beginning of the plastic deflection, when the phenomenon of yield strength starts. In this area, a gradual decline of the induced electromotive force can be observed, what is related to the decline of the steel bar section. Finally, in the last part of the graphics, there is a rapid increase of the slope of the curve corresponding to the moment of the break. That finishes with the sample divided into two parts.

3.3. Variation of magnetic behaviour of the sample in relation to the applied force

This study also determines the variation of the magnetic permeability of B500-SD steel specimens, for different tensile states under different magnetic induction states. For the measuring of magnetization field H, a Hall probe was used. It was also examined the effects of uniaxial tensile strength in the cycles of hysteresis of 12 mm and 16 mm diameter steel bars.

As illustrated in Figure 9 and Figure 10, we see the behaviour within a tension range from 0 to 60 kN in intervals of 15 kN for 12 mm diameter bars, and within a tension range from 0 to 120 kN in steps of 20 kN for 16 mm diameter bars. Two similar behaviours can be observed, as on the one hand, the maximum permeability decreases when the applied tensile force increases, and on the other, the maximum point of permeability shifts to the right for higher magnetic fields. Moreover, it can be also observed how the permeability is higher for bars with a larger diameter.

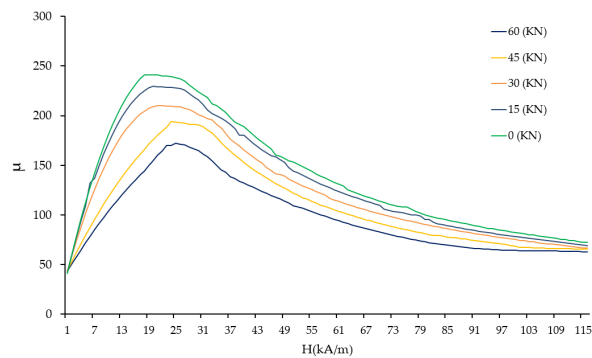


FIGURE 9. Permeability - Magnetic induction (kA/m) under different stress levels before the rupture. B500-SD steel bar of 12 mm diameter.

The measuring equipment and the described method allow ascertaining effectively the elastic limit of a steel bar as well as its tensile state under a specific load. The latter is of particular relevance concerning bars that are embedded into reinforced concrete structures and it is impossible to reach them without destroying the containing surface.

Finally, as it can be seen in Figure 11a, figure that was obtained from an infrared thermography using a FLIR E50 bx camera, during the tensile test, there is an overheating of the bar. This overheating is enhanced as we approach the point of rupture. This thermographic inspection allows regulating the position of the coils during the test, placing their centre into the point of rupture where the variation of the magnetization is studied. Moreover, Figure 11b and 11c shows the final state of a bar of B500SD steel and diameter 16 mm after the rupture. The analysis of its final temperature shows that even though this final temperature is higher than the ambient temperature, it is lower than the temperature of the change on its magnetic properties (normally about 230°C for carbon steels) (29).

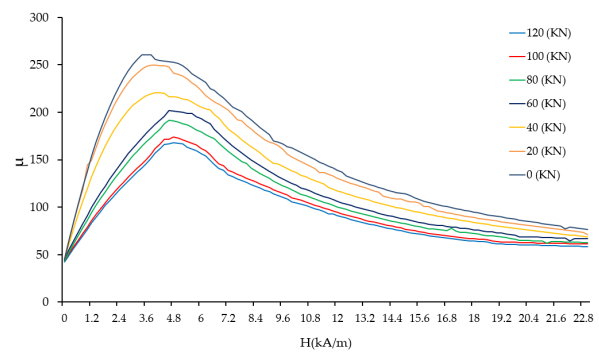


FIGURE 10. Permeability - Magnetic induction (kA/m) under different stress levels before the rupture. B500-SD steel bar of 16 mm diameter.

4. CONCLUSIONS

The study of the magnetic behaviour of steel is a useful alternative method to obtain different mechanical behaviour and the yielding limit of steel under tensile stress. This research presents a measuring equipment able to register, through the variation of induced electromotive force, the rates of tension and deflection of construction steel B500-SD during a tensile test. Two commercial diameters of bars used in the building were implemented: 12 mm and 16 mm. The measurement method presented in this work could serve as a starting point to develop new sensors and equipment to determine the stress state of steel bars embedded in structural concrete without the necessity to extract it and test it in the laboratory. These techniques of inspection are of great technical interest for building assessments.

The magnetic test provides practical and valuable information for the evaluation of construction steel properties in its future mechanical uses. It was possible to verify how, as the applied axial tensile strength increases, the maximum magnetic

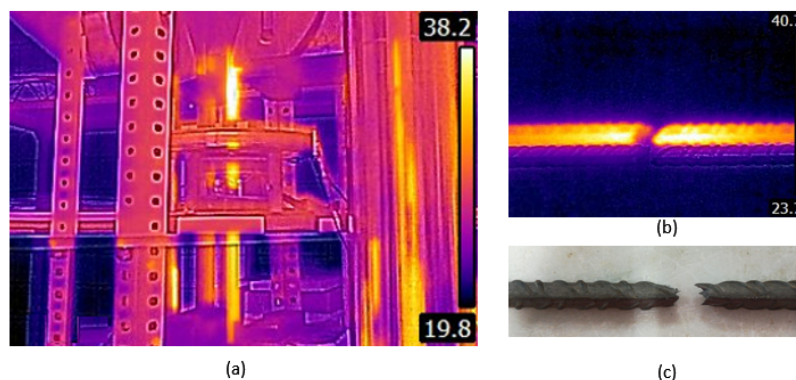


FIGURE 11. (a) Infrared Thermography during tensile test; (b) Thermography of B500SD after standardized tensile test; (c) Final state of B500SD bar of 16 mm after the rupture.

permeability of the steel decreases. Moreover, when the tensile force rises, the magnetic field to be applied in order to obtain the maximum permeability of the material also increases. Finally, infrared thermography confirms that the force applied to the specimen gets transformed into deflection work, and a small part is used for sample heating.

ACKNOWLEDGMENTS

Authors appreciate the collaboration of the professor Álvaro Gustavo Vitores González of the *Escuela Técnica Superior de Ingeniería y Diseño Industrial* of Madrid for the theoretical development of this paper.

REFERENCES

- Senobua, A. J.; Garzón, E.; Ayuso, J.; Perez, F.; Caballero, A. (2003) Characterizing of steel used in the construction of civil works in Almería. *Rev. Metal.* 39, 461-468. ISSN: 1988-4222.
- Wu, W.; Yin, H.; Zhang, H.; Kang, J.; Li, Y.; Dan, Y. (2018) Electrochemical investigation of corrosion of X80 steel under elastic and plastic tensile stress in CO₂ environment. *Metals.* 8 [11], 949. <https://doi.org/10.3390/met8110949>.
- Watarai, H.; Fan, R.; Yang Liu, J.; Djauhari, J. (2018) Falling velocity magnetometry of ferromagnetic microparticles. *J. Magn. Magn. Mater.* 462, 22-28. <https://doi.org/10.1016/j.jmmm.2018.04.045>.
- Bao, S.; Fu, M.; Lou, H.; Bai, S. (2017) Defect identification in ferromagnetic steel based on residual magnetic field measurements. *J. Magn. Magn. Mater.* 441, 590-597. <https://doi.org/10.1016/j.jmmm.2017.06.056>.
- Wang, G.; Wang, X.; Liao, Y. (2019) Theoretical investigation on the ferromagnetic two-dimensional scandium monochloride sheet that has a high Curie temperature. *Appl. Surf. Sci.* 471, 1011-1016. <https://doi.org/10.1016/j.apsusc.2018.12.109>.
- Deng, D.; Wu, X. (2018) Feasibility study of determining axial stress in ferromagnetic bars using reciprocal amplitude of initial differential susceptibility obtained from static magnetization by permanent magnets. *J. Magn. Magn. Mater.* 449, 243-256. <https://doi.org/10.1016/j.jmmm.2017.10.039>.
- Petković Dejan, M.; Radić Milica, D. (2015) Generalization of Helmholtz Coil Problem. *Serbian J. Electr. Engineer.* 12 [3], 375-384. <https://doi.org/10.2298/SJEE1503375P>.
- Rubel Basar, Md.; Yazed Ahmad, M.; Cho, J.; Ibrahim, F. (2016) An improved resonant wireless power transfer system with optimum coil configuration for capsule endoscopy. *Sen. Actuat. A: Phys.* 249, 207-216. <https://doi.org/10.1016/j.sna.2016.08.035>.
- Fano, W. G.; Alonso, R.; Quintana, G. (2017) El campo magnético generado por las bobinas de Helmholtz y sus aplicaciones a calibración de sondas. *Elektron.* 1 [2], 91-96. <https://doi.org/10.37537/rev.elektron.1.2.25.2017>.
- Clayton, R.P. (2005) Introduction to electromagnetic compatibility (EMC), Second Edition. Hoboken, N. J. Wiley-Interscience, New Jersey, (2006). <https://doi.org/10.1002/0471758159>.
- Deng, D.; Wu, X. (2018) Feasibility study of determining axial stress in ferromagnetic bars using reciprocal amplitude of initial differential susceptibility obtained from static magnetization by permanent magnets. *J. Magn. Magn. Mater.* 449, 243-256. <https://doi.org/10.1016/j.jmmm.2017.10.039>.
- Shi, Y.; Zhang, C.; Li, R.; Cai, M.; Jia, G. (2015) Theory and application of magnetic flux leakage pipeline detection. *Sensors.* 15 [12], 31036-31055. <https://doi.org/10.3390/s151229845>.
- Ge, J.; Li, W.; Chen, G.; Yin, X.; Yuan, X.; Yang, W.; Liu, J.; Chen Y. (2017) Multiple type defect detection in pipe by Helmholtz electromagnetic array probe. *NDT E Int.* 91, 97-107. <https://doi.org/10.1016/j.ndteint.2017.07.001>.
- Suresh, V.; Abudhahir, A.; Daniel, J. (2017) Development of magnetic flux leakage measuring system for detection of defect in small diameter steam generator tube. *Measurement.* 95, 273-279. <https://doi.org/10.1016/j.measurement.2016.10.015>.
- Ramírez Fernández, P. (2015) Cinética de dominios de sistemas magnéticos. Aplicación al desarrollo de sensores magnéticos. Universidad Politécnica de Madrid, Tesis Doctoral.
- Xiucheng, L.; Donghang, W.; Cunfu, H.; Huan, F.; Bin, W. (2018) Comparison of AC and pulsed magnetization-based elasto-magnetic methods for tensile force measurement in steel strand. *Measurement.* 117, 410-418. <https://doi.org/10.1016/j.measurement.2017.12.033>.
- Xiucheng, L.; Wanli, S.; Cunfu, H.; Ruihuan, Z.; Bin, W. (2018) Simultaneous quantitative prediction of tensile stress, surface hardness and case depth in medium carbon steel rods based on multifunctional magnetic testing techniques. *Measurement.* 128, 455-463. <https://doi.org/10.1016/j.measurement.2018.04.044>.
- Thring, C.B.; Fan, Y.; Edwards, R.S. (2016) Focused Rayleigh wave EMAT for characterisation of surface-breaking defects. *NDT E Int.* 81, 20-27. <https://doi.org/10.1016/j.ndteint.2016.03.002>.
- Ashigwuike, E.C.; Ushie, O.J.; Mackay, R.; Balachandran, W. (2015) A study of the transduction mechanisms of electromagnetic acoustic transducers (EMATs) on pipe steel materials. *Sen. Actuat. A: Phys.* 229, 154-165. <https://doi.org/10.1016/j.sna.2015.03.034>.
- Xu, J.; Xiong, H.; Wu, X. (2011) Signal processing for the guided wave test based on the empirical mode decomposition. *International Conference on Electrical and Control Engineering*, 1233-1240.
- Reitz, J. R.; Milford, F. J. (2001) Fundamentos de la teoría electromagnética. Editorial Alhambra, S. A. Madrid (2001).
- UNE-EN ISO 6892-1:2017. (2017) Materiales metálicos. Ensayo de tracción. Parte 1: Método de ensayo a temperatura ambiente. AENOR (2017).
- Suárez Guerra, F. (2013). Estudio de la rotura en barras de acero: aspectos experimentales y numéricos. Tesis Doctoral, E.T.S.I. Caminos, Canales y Puertos (UPM).
- Ulaby, F. T.; Ravaioli, U. (2017) Fundamentals of Applied Electromagnetics (7th Edition). Pearson, Londres (2017).
- Zhu, Z.; Sun, G.; He, C.; Liu, A. (2018) Prediction of the tensile force applied on surface-hardened steel rods based on a CDIF and PSO-optimized neural network. *Meas. Sci. Technol.* 29 [11], 115602. <https://doi.org/10.1088/1361-6501/aadebf>.
- Kvasnica, B.; Fabo, P. (1996) Highly precise non-contact instrumentation for magnetic measurement of mechanical stress in low-carbon steel wires. *Meas. Sci. Technol.* 7, 763-767.
- William D.; Callister, Jr. (2012) Materials Science and Engineering. An Introduction. Third Edition. Editorial Reverte, vol. 2. Barcelona (2012).
- Lorenzo, L. (2017) Ciencia de Materiales. Servicio de Publicaciones, Escuela Técnica Superior de Ingeniería y Diseño Industrial, Departamento de mecánica industrial. Universidad Politécnica de Madrid (2017).
- Reina, M. (2012) Soldadura de los aceros y aplicaciones. Editorial Weldwork, S. L. 5ª Edición, Madrid (2012).